Journal of Applied Electrochemistry (2006) 36:463–474
DOI 10.1007/s10800-005-9100-0
© Springer 2005

Photoelectrochemical characterisation of thermal and particulate titanium dioxide electrodes

I. MINTSOULI, N. PHILIPPIDIS, I. POULIOS and S. SOTIROPOULOS*
Department of Chemistry, Aristotle University of Thessaloniki, Thessaloniki 54124, Greece
*(*author for correspondence, tel.: +30-2310-997742, fax: +30-2310-443922, e-mail: eczss@chem.auth.gr)*

Received 31 May 2005; accepted in revised form 4 November 2005

Key words: particulate electrodes, photoelectrochemistry, thermal electrodes, titanium dioxide

Abstract

The photoelectrocatalytic performance of thermal and particulate TiO_2 films on Ti electrode substrates has been studied by photovoltammetry and bulk photoelectrolysis. The thermal TiO_2 film electrodes were prepared by Ti annealing in air at 700 °C and 500 °C while the particulate electrodes were prepared from dispersions of Degussa P-25 TiO_2 deposited onto Ti substrates and subsequently sintered at 700 °C and 500 °C. The photocurrent in the absence and presence of the model organic species of oxalate as well as its photooxidation rate depends on coating surface area, type (thermal or particulate) and crystallographic form (anatase or rutile). A method is proposed to account for surface area variations by normalising the data with respect to the electroactive surface area of the TiO_2 electrodes, as estimated by their surface electrochemistry in the dark. The thermal electrodes show high photocurrents both in the absence and the presence of oxalate whereas the performance of particulate electrodes is significantly improved upon oxalate addition. Nevertheless, the efficiency of thermal 700 °C TiO_2 for oxalate photooxidation during bulk photoelectrolysis is comparable to that of Degussa P-25 TiO_2-coated electrodes.

1. Introduction

The use of supported TiO_2 photocatalysts for water treatment instead of catalyst slurries offers some advantages namely, the absence of the costly step of catalyst removal and a modular design of the treatment cell [1–3]. On the other hand, drawbacks of supported catalysts include their small total surface area and mass transport limitations. To overcome these, TiO_2 can be supported on an electronic conductor and biased positive with the application of an external voltage in an appropriate electrochemical cell, so that the rate of photogenerated electron and hole recombination is limited and the rate of surface reactions increased (electrically enhanced photocatalysis) [4–7].

The majority of TiO_2 photocatalytic electrodes suggested for decontamination applications are of a particulate nature i.e. they are made of TiO_2 nanoparticles further aggregated to micrometer-sized particles during thermal annealing. The catalyst layer is either synthesised in the laboratory by a variety of methods [8–18] or, alternatively, prepared from commercial Degussa P-25 TiO_2 suspensions by dip-coating, spraying or sedimentation techniques [19–21].

Most particulate TiO_2 electrodes are either anatase or mixtures of anatase–rutile while there are only a few electrophotocatalytic studies of particulate laboratory-made rutile electrodes [4, 7, 22, 23] and none of commercial Degussa P-25 transformed to rutile by high temperature annealing. At the same time, continuous TiO_2 film electrodes produced by simple thermal annealing have also not often been used in photooxidation applications [4, 7, 23]. Finally, despite many studies of TiO_2 electrochemistry in the dark [24–27], the Ti(III)/Ti(IV) surface electrochemistry at potentials positive to hydrogen evolution has not been correlated to its performance under UV illumination.

The aim of this work was to carry out a comparative study of thermal and particulate TiO_2 photoelectrodes (of the anatase and/or rutile type) with respect to their electrochemistry in the dark and under UV illumination, in order to distinguish the effects of film morphology, surface area and crystal structure. The main objectives have been: (a) the electrochemical characterisation of the photoelectrodes in the dark by means of cyclic voltammetry, in order to obtain an estimate of electroactive area from their surface electrochemistry and use that for normalisation of their photoactivity with respect to surface area variations; (b) their photoelectrochemical characterisation in the supporting electrolyte and in the presence of organics by means of photovoltammetry; and (c) the correlation of electrode type and photocurrent characteristics with the efficiency of organics photodegradation during bulk photooxidation experiments.

2. Experimental

2.1. *Preparation of thermal and particulate TiO_2 coatings on Ti electrode substrates*

Ti specimens (1 cm×0.5 cm for voltammetry and 10 cm×10 cm for bulk photoelectrolysis) were cut from 0.5-mm thick plates and were etched for a few seconds in a HF/HNO_3 3:1 mixture before washed thoroughly with doubly distilled water. The thermal film electrodes (T-TiO_2) were prepared by annealing the etched Ti substrates in air at 700 °C (for 5 h) or 500 °C (for 1.5 h) in a Carbolite CWF 1100 oven. The particulate electrodes (P-TiO_2) were prepared by spraying or sedimentation on one side of the substrate from a 1 g l^{-1} methanol dispersion of Degussa P-25 TiO_2 onto the Ti substrates, evaporating methanol at 50 °C for 10 min, repeating the procedure for 10 times and finally sintering in air at 700 °C (for 5 h) or 500 °C (for 1.5 h). Very thick films of particulate TiO_2 were thus produced having a loading in the 10–20 mg cm^{-2} range and a thickness in the 25–50 μm range. The long annealing period of 5 h at 700 °C was found necessary to produce uniform thermal rutile films (times longer than 3 h were needed) and, mainly, to fully convert P-25 particulate films into their rutile form.

Locations on the backside of the electrodes were etched again (to remove oxides formed during annealing) and insulated Cu wire was glued onto them with silver-loaded epoxy resin (RS). Finally, the contact as well as the entire back side of the electrode were insulated with epoxy resin glue (RS).

2.2. *Microscopic and XRD characterisation of TiO_2 layers*

Scanning Electron Microscopy (SEM) was carried out using an JSM 733 microscope.

X-ray diffraction (XRD) deposit characterisation was performed with the help of a Rigakou Miniflex diffractometer.

2.3. *Photoelectrochemical characterisation of TiO_2 coatings*

Cyclic voltammetric and constant potential experiments on TiO_2 electrodes in the dark and under UV illumination were carried out with the Autolab 30 (EcoChimie) system in a three-electrode cell equipped with a flat quartz window opposite the working electrode. A saturated calomel electrode (SCE) was used as the reference electrode and a Pt foil as the counter electrode. Voltammograms were run for at least three consecutive full cycles since preliminary experiments showed that a near-steady state response was observed only after the second run; all results reported correspond to the stabilised voltammetric picture. Also, due to the enhancement of the photocurrent upon electrode exposure in the hydrogen evolution region (negative to −0.9 V vs. SCE), the starting potential for all voltammograms was −1.1 V vs. SCE even if not shown in the figures. This effect is in accordance with the well-known increase in TiO_2 donor density upon its reduction by high temperature annealing in H_2 (or in general, in reductive environments) or by electrochemical cathodisation in the hydrogen evolution region [28].

A Radium Ralutec 9W/78 UVA lamp ($\lambda = 350$–400 nm, $\lambda_{max} = 366$ nm), placed at a distance of 2.5 cm from the sample, was used for front face electrode illumination. The power density on the sample surface position was measured as 3 mW cm^{-2} with a photometer.

2.4. *Bulk photo-oxidation of oxalate at UV-illuminated Ti/TiO_2 electrodes*

A 500-ml cylindrical cell with a removable cap has been used. The UV lamp, placed in a cylindrical sleeve, was introduced from an opening in the middle of the cap leaving a solution available volume of 300 ml. Samples of 2 ml were taken with the help of a tubing and oxalate was determined by titration with permanganate. Rectangular ca. 100 cm^2 Ti/TiO_2 electrodes were used; they were bent into a hemicylindrical shape and inserted in the cell with their back side touching the cell walls and their active side facing the lamp. A stainless steel wire was used as the counter electrode and the reference electrode was a SCE electrode equipped with a salt bridge made of a thin thermoplastic tube ending to a Vycor® tip.

2.5. *Electrode materials and chemicals*

Ti plates 0.5 mm thick were from Alfa Aesar (99.5%, metals basis). The supporting electrolyte was prepared from K_2SO_4 (Merck, pro analysi, >99%) or Na_2SO_4 (Merck, pro analysi, >99%) (no significant dependence of the results on cation type was observed). Potassium oxalate was obtained from Fluka, (>99.5% (RT)) and potassium permanganate from Merck (>99%) was used for its titration. Doubly distilled water was used for the preparation of solutions and all experiments were carried out at room temperature.

3. Results and discussion

3.1. *Microscopic and structural characterisation of TiO_2*

Figure 1(a) and (b) show SEM micrographs of the surface of T-TiO_2 (500 °C) and T-TiO_2 (700 °C) thermal electrodes; the surface is characterised by large patches of 10–20 μm polyhedra, resulting from Ti etching prior to thermal treatment. Figure 1(c) and (d) depict the surface of P-TiO_2 (500 °C) and P-TiO_2 (700 °C) particulate electrodes, characterised by a network of spherical few μm-sized aggregates into which the tens of nm-sized P-25 particles have merged, following annealing. No

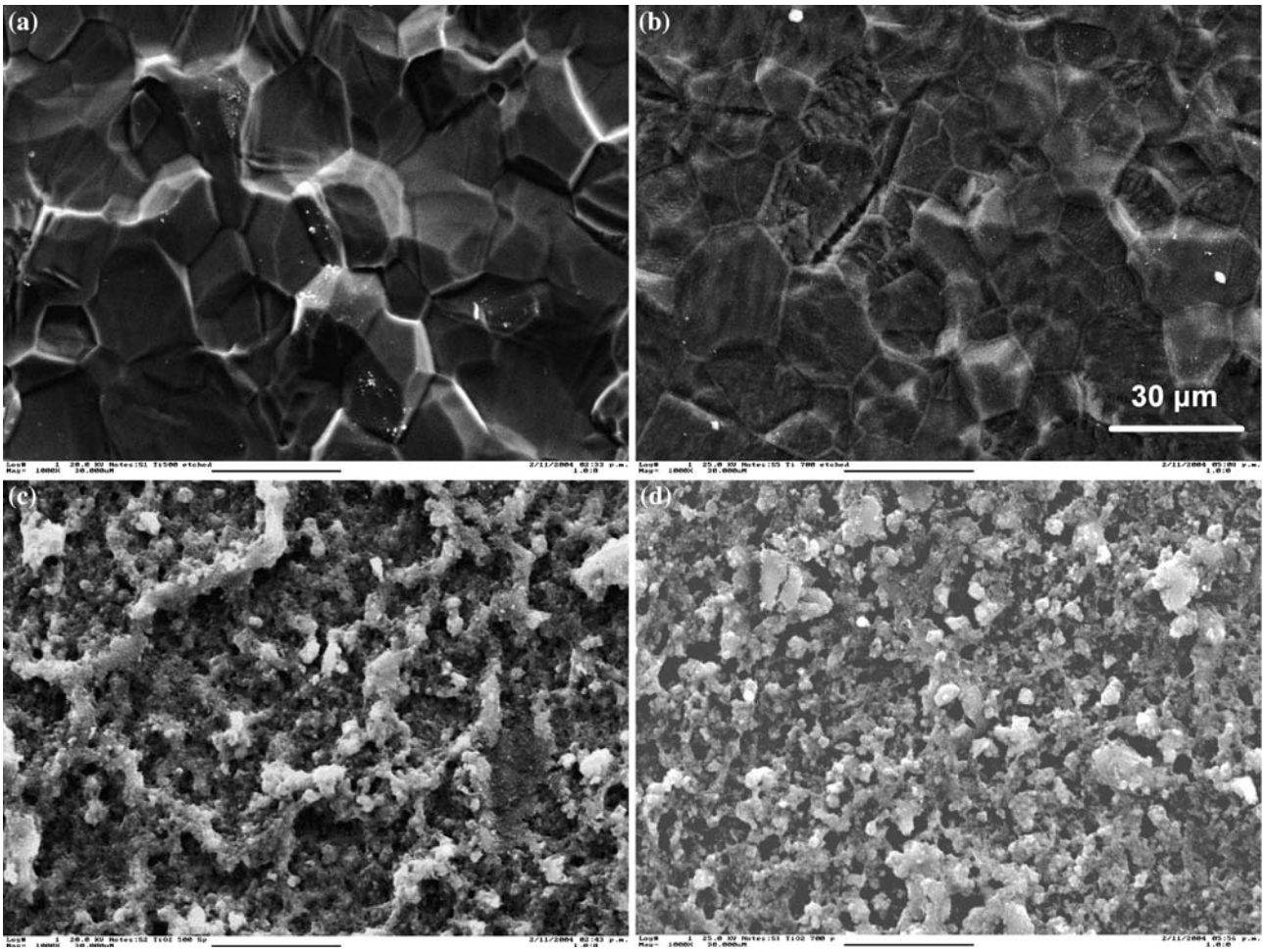

Fig. 1. SEM micrographs (at magnification indicated by the scale bar in (b)) of (a) T-TiO_2 (500 °C) and (b) T-TiO_2 (700 °C) thermal electrodes and (c) P-TiO_2 (500 °C) and (d) P-TiO2 (700 °C) particulate electrodes.

striking difference in film morphology for the particulate electrodes can be inferred from the SEM picture. Thermal films prepared at 500 °C and 700 °C were confirmed by XRD to be pure anatase and rutile, respectively. Particulate films annealed at 500 °C retained the P-25 anatase to rutile percentage composition (80% ÷ 20%) while those annealed at 700 °C were converted to pure rutile.

3.2. *Electrochemical characterisation of TiO_2 coatings in the dark*

This was carried out by fast (100 mV s^{-1} potential scan rate) cyclic voltammetric experiments in the dark, in order to establish the electrochemically active surface area of the TiO_2 electrodes. The method is based on the surface reaction of the Ti(IV)/Ti(III) transformation that is known to occur at potentials negative to the flat band potential of TiO_2 and just prior to hydrogen evolution [24–27]. Figure 2(a) presents characteristic cyclic voltammograms in 1 M Na_2SO_4 solutions for the T-TiO_2 (500 °C) and T-TiO_2 (700 °C) electrodes and Figure 2(b) the corresponding curves for the particulate electrodes. All electrodes show a couple of cathodic and anodic main peaks (with a couple of ill-defined small peaks in their foot at more positive potentials) prior to hydrogen evolution, corresponding to the reduction and oxidation transformations of the Ti(IV)/Ti(III) couple on the surface of the films. The reduction and re-oxidation of Ti surface species can be formulated for TiO_2 in general as [26]:

$$\mathrm{Ti(IV)} + \mathrm{e^-} \leftrightarrow \mathrm{Ti(III)} \tag{1}$$

and has been formulated for anatase as [25]:

$$^{*}(\mathrm{Ti^{4+}})_4(\mathrm{O^{2-}})_8 + \mathrm{H_2O} + \mathrm{e^-} \leftrightarrow \mathrm{H^+}(\mathrm{Ti^{3+}})(\mathrm{Ti^{4+}})_3(\mathrm{O^{2-}})_8 + \mathrm{OH^-} \tag{2}$$

(where * denotes vacant octahedral sites).

The peaks varied linearly with scan rate and the charge of the cathodic peak was estimated as 7.7 mC cm^{-2} for the P-TiO_2 (500 °C) electrode and 5.7 mC cm^{-2} for the P-TiO_2 (700 °C) one, whereas as 0.26 mC cm^{-2} and 0.16 mC cm^{-2} for the T-TiO_2 (700 °C) and T-TiO_2 (500 °C) electrodes, respectively. These charge densities are translated to the modest electroactive surface area-per-geometric area (roughness factor) values of 53.5, 39.6, 1.8 and 1.1 cm^2 cm^{-2}, respectively, taking into account that 9 Ti^{4+} ions nm^{-2} is the Ti ion surface

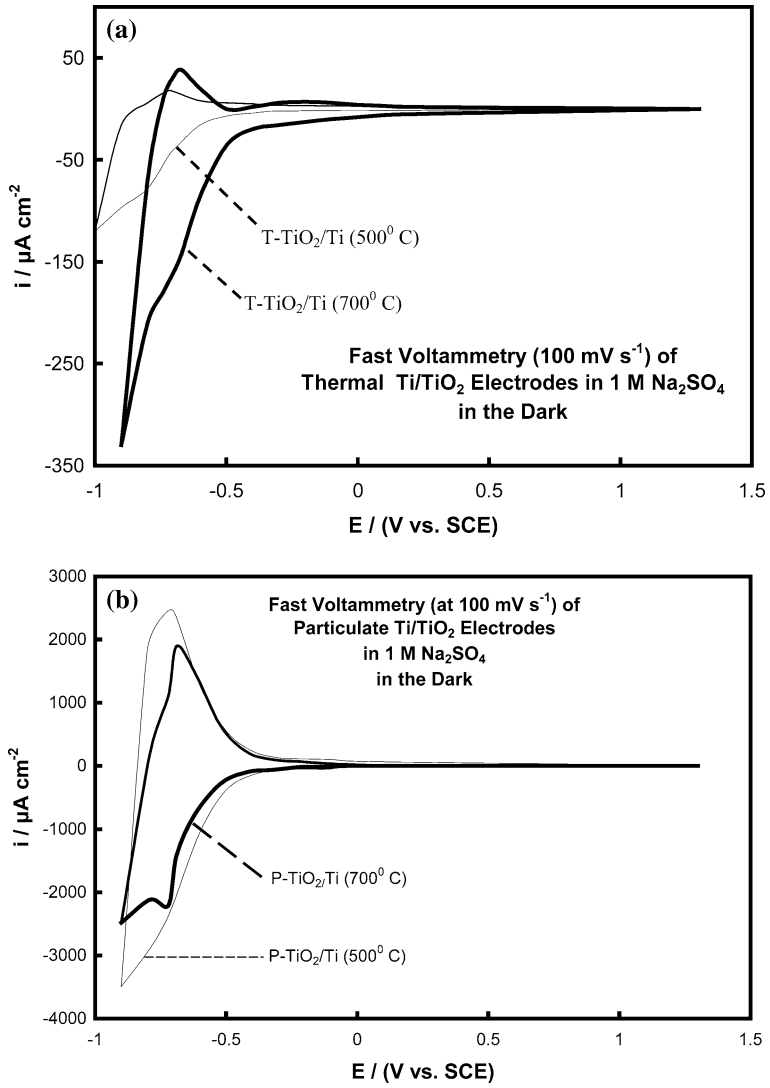

Fig. 2. Voltammograms of thermal (a) and particulate (b) TiO_2/Ti electrodes (as indicated in the graph) recorded at a 100 mV s^{-1} potential scan rate in the dark, in deaerated solutions of 1 M Na_2SO_4.

density of a typical TiO_2 crystal structure [29] and hence the Ti(IV)/Ti(III) transformation is associated with a 144 μC cm^{-2} charge density. It follows that, in accordance with reported surface area data for TiO_2 particles, the anatase rich particulate film has a higher electroactive area than the rutile one (which was also sintered at a higher temperature). The higher electroactive surface area of the thermal rutile film from that of the thermal anatase may be attributed to the formation of a rougher thermal oxide (as inferred from the SEM photographs of Figure 1(a) and (b)).

Despite the wide loading and thickness variation (loading in the 10–20 mg cm^{-2} range and a thickness in the 25–50 μm range) of the crudely produced (by spraying or sedimentation) particulate films, the charge density variation showed no clear trend and was limited in the 6–8 mC cm^{-2} range for P-TiO_2 (500 °C) electrodes and in the 4–6 mC cm^{-2} range for the P-TiO_2 (700 °C) ones. Thus, the magnitude and shape of the surface electrochemistry peaks did not depend on TiO_2 loading and thickness of the particulate films in a manner other than that due to morphological surface variations between different electrode batches (at least for these loading levels). This indicates that only the topmost porous layers were accessible to the electrolyte and that no significant ohmic losses were introduced by the film (at least in the negative to the flatband potential, "metallisation", region).

3.3. *Photoelectrochemical characterisation of TiO_2 coatings*

3.3.1. *Experiments in supporting electrolyte*

Figure 3 shows indicative photocurrent vs. potential curves (recorded at 10 mV s^{-1}) at various TiO_2 electrodes in deaerated 1 M Na_2SO_4 solutions, under UV illumination (360 nm, 3 mW cm^{-2}). In the absence of oxidisable species this current is a measure of $OH^{\cdot}$ radicals (and other primary oxidation products such as

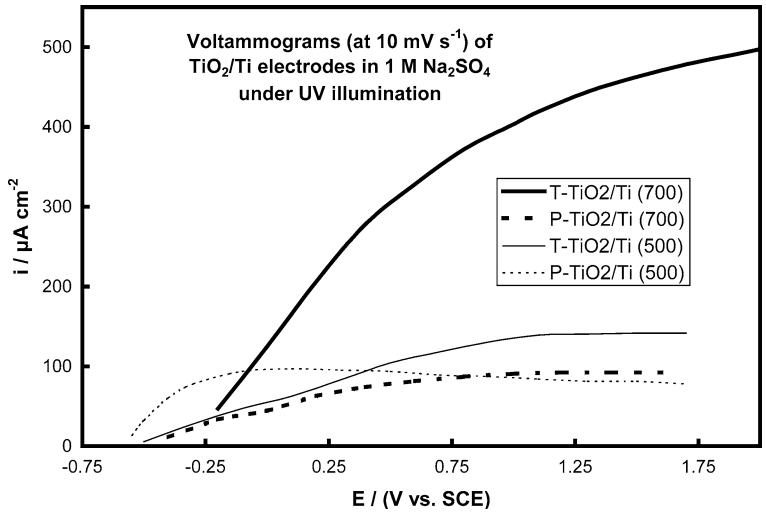

Fig. 3. Photovoltammograms of thermal and particulate TiO_2/Ti electrodes (as indicated in the graph) recorded at a 10 mV s^{-1} potential scan rate under UV illumination, in deaerated solutions of 1 M Na_2SO_4.

$O_2^{\cdot-}$ and H_2O_2) produced at the electrode surface from water oxidation by photogenerated holes. The photocurrent tends to a limiting value at high positive potentials where it is determined by migration or diffusion of charge carriers in the semiconductor films (depending on whether these were continuous [30, 31] or particulate [32–34]). For electrodes annealed at 500 °C (anatase-rich) the onset potential of the photocurrent (which can be approximated to the flat band potential) is lower than that for 700 °C electrodes (rutile-rich), in accordance with the flatband potential of anatase reported to be more negative than that of rutile [35].

The magnitude of the limiting current is a measure of the overall electro-photocatalytic performance of an electrode which is determined by (i) its inherent, open-circuit photocatalytic activity; (ii) its surface area and electroactive area; and (iii) the electric field enhancement (suppression of recombination) effect. The first and second parameters are expected to depend on the structure (anatase or rutile) and form (thermal or particulate; particle size), whereas the third one on the form and conductivity of the electrode.

Table 1 presents the observed photocurrent densities per nominal area (i_{ph}) and the corresponding incident photon-to-current efficiency, IPCE. The latter is given by the expression [36]:

$$\mathrm{IPCE}\% = 100\frac{1240 i_{ph}}{\lambda P} \tag{3}$$

where i_{ph} is the photocurrent in mA cm^{-2}, λ the wavelength of the incident light in nm and P the incident light intensity in mW cm^{-2}. The ICPE value of the thermal electrode of 700 °C (ca. 55%) is remarkably high for a plain supporting electrolyte solution while the values for the other electrodes are of the expected magnitude (still, higher than recently reported values for particulate electrodes in the absence of organics [37]).

Based on the results of Figure 3, the trend of the observed photocurrent density per nominal area, i_{ph}, at +1.7 V vs. SCE in the absence of organics is:

$$\begin{aligned}&\text{T-TiO}_2(700\ ^\circ\text{C}) >> \text{T-TiO}_2(500\ ^\circ\text{C})\\ &> \text{P-TiO}_2(700\ ^\circ\text{C}) > \text{P-TiO}_2(500\ ^\circ\text{C}).\end{aligned} \tag{4}$$

The rationalisation of any such trend may be complicated as it should be done in terms of a number of parameters that affect the photocurrent to different extents and sometimes in opposite directions: thermal films (especially those prepared at higher temperatures) have been reported to show high electro-photocatalytic activity towards the oxidation of water [7, 38]; anatase particles have a higher surface area and higher

Table 1. Ti(IV)/Ti(III) reduction charge density, q, roughness factor, r, photocurrent density at +1.7 V vs. SCE per geometric area, i_{ph}, photocurrent density at +1.7 V vs. SCE per electroactive area, i'_{ph}, incident-photon-to-current efficiency, IPCE and photocurrent enhancement factor (upon oxalate addition), F, for thermal (T) and particulate (P) TiO_2/Ti photoelectrodes in 1 M Na_2SO_4 and 0.01 M oxalate + 1 M Na_2SO_4 solutions

	q (mC cm^{-2})		1 M Na_2SO_4			0.01 M oxalate + 1 M Na_2SO_4			F
		r	i_{ph} (μA cm^{-2})	IPCE (%)	i'_{ph} (μA cm^{-2})	i_{ph} (μA cm^{-2})	IPCE (%)	i'_{ph} (μA cm^{-2})	
T-TiO_2 (700 °C)	0.26	1.8	478	54.9	265.5	470	54.0	261.1	0.98
P-TiO_2 (700 °C)	5.70	40	90	10.3	2.3	160	18.4	4.0	1.78
T-TiO_2 (500 °C)	0.16	1.1	142	16.3	129.1	163	18.7	148.2	1.15
P-TiO_2 (500 °C)	7.70	54	78	8.96	1.5	397	45.6	7.4	5.09

open-circuit photocatalytic activity towards the oxidation of organics than rutile particles [39] but the latter are known to be better photoelectrocatalysts for water oxidation; particulate films have higher surface areas than thermal ones but, due to small particle size and absence of a depletion layer, are less affected by the application of an electric field [32–34].

The electroactive area of the TiO_2 electrode (calculated from its surface electrochemistry in the dark) should be directly related to its photo-electrochemically active surface area, since they both refer to TiO_2/electrolyte sites affected by the application of the electric field. Hence, to account for differences in electroactive surface area between different electrode types (as well as to remove the effect of sample variations between different batches), the photocurrent can be normalised with respect to that area, defining a photocurrent density per electroactive area, i'_{ph}. Table 1 presents the observed photocurrent densities per nominal area (i_{ph}), charge densities of the Ti(IV)/Ti(III) transformation in the dark (q) and associated roughness factors (r), as well as the photocurrent densities per electroactive area (i'_{ph}) for all types of electrodes tried. The trend of the observed i'_{ph}, at +1.7 V vs. SCE in the absence of organics becomes:

$$\text{T-TiO}_2(700\ ^\circ\text{C}) > \text{T-TiO}_2(500\ ^\circ\text{C}) >> \text{P-TiO}_2(500\ ^\circ\text{C}) > \text{P-TiO}_2(700\ ^\circ\text{C}), \quad (5)$$

further stressing the higher electric field enhancement effect on the continuous thermal films.

Figure 4(a) and (b) show plots of the square of the photocurrent, i^2_{ph}, obtained from the voltammograms of Figure 3, with respect to the applied potential, E, for the thermal electrodes. These plots show reasonable linearity in an extended potential range of 1.2 V in the case of thermal films, as expected for semiconductor layers

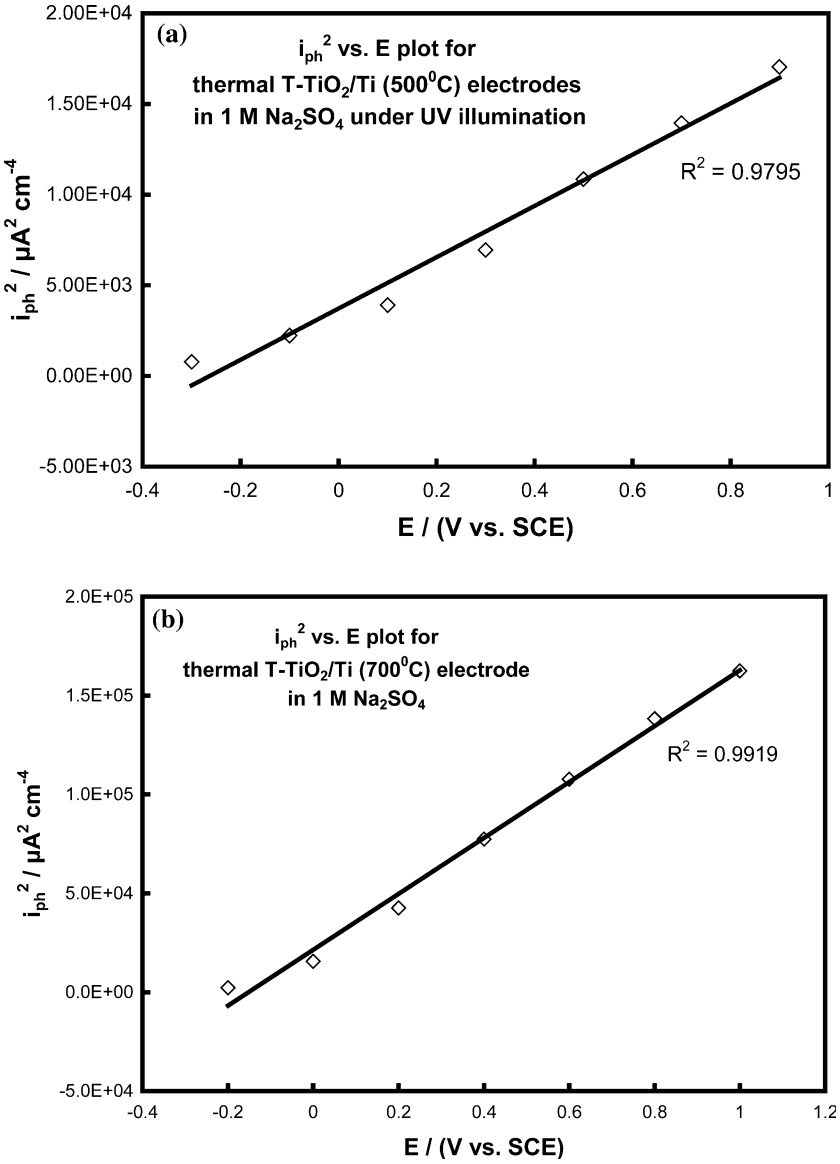

Fig. 4. Plots of the photocurrent densities at +1.7 V vs. SCE (estimated from the photovoltammograms of Figure 3) to the square, i^2_{ph}, with electrode potential, E, for T-TiO_2/Ti (500 °C) (a) and T-TiO_2/Ti (700 °C) (b) thermal electrodes.

thick enough for a depletion layer to be developed [30, 31]. In contrast, no reasonable linearity over an appreciable potential range was obtained for the particulate electrodes: the small particle size of the coatings means that no depletion layer is formed and that charge carrier transport occurs by diffusion [32–34].

3.3.2. *Experiments in the presence of organics*

The rate of photogenerated $OH^{\cdot}$ in supporting electrolyte solutions does not determine on its own the rate of organics photodegradation. This is because (a) the radicals may not be fully utilised for the indirect oxidation of the organics but they can also react with each other to give hydrogen peroxide and finally oxygen and (b) there may also be a hole uptake (direct oxidation) mechanism of the organic. Hence, photovoltammetric experiments were also carried out in 1 M Na_2SO_4 solutions containing the model organic species of oxalate at 0.001–0.1 M levels. Figure 5(a–d) show photovoltammograms in the absence (1 M Na_2SO_4) and presence (+0.01 M oxalate) of oxalate for all types of electrodes studied. The largest increase in photocurrent with the addition of the organic was observed for the particulate films and, among electrodes of the same type, for anatase-rich samples. There was very little increase for the thermal films and, in fact, a slight decrease in the case of the thermal rutile electrode T-TiO_2 (700 °C). The increase in the limiting photocurrent in the presence of organics is an indication of their direct oxidation by hole uptake following adsorption on the electrode surface and it has already been postulated for oxalate [40, 41]. This could be one of the reasons why the effect is more pronounced on particulate and anatase-rich films due to their higher surface area and adsorption capacity. However, the main reason for the pronounced effect of oxalate on particulate electrodes should be their ability to act as efficient hole scavengers in a system that the electric field has a limited action and recombination rates are otherwise high. A quantification of the oxalate effect on the photocurrent can be made based on the

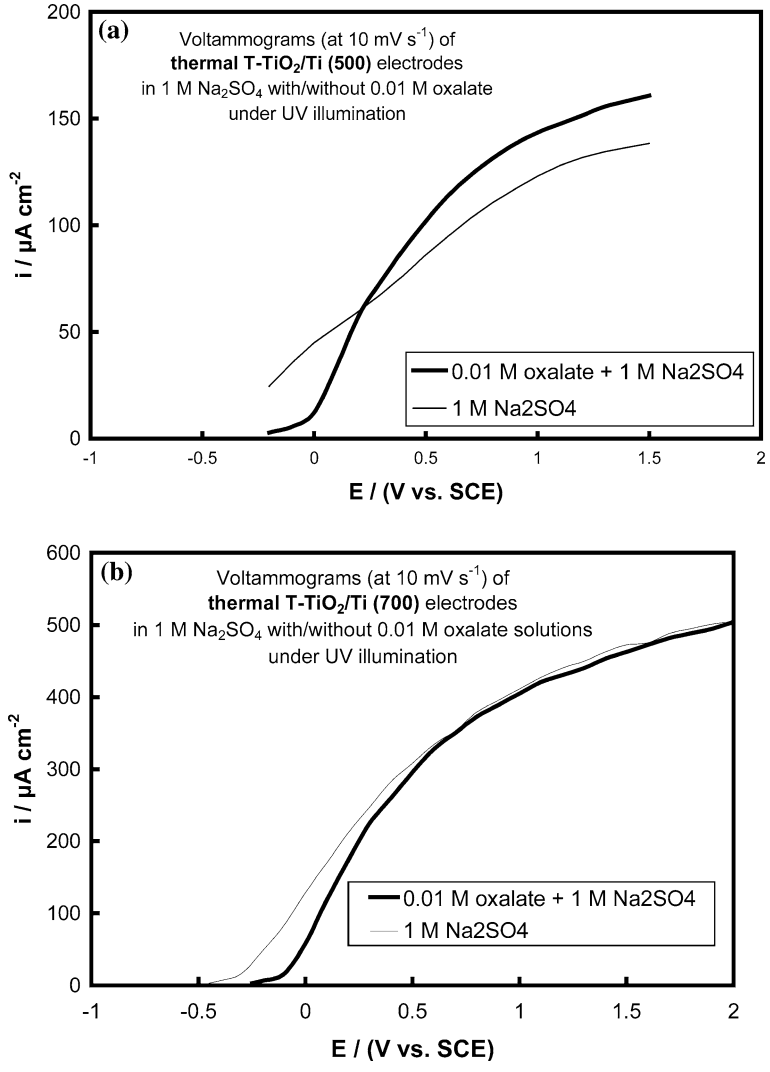

Fig. 5. Photovoltammograms of TiO_2/Ti electrodes recorded at a 10 mV s^{-1} potential scan rate under UV illumination, in deaerated solutions of 1 M Na_2SO_4 and 0.01 M oxalate + 1 M Na_2SO_4, for (a) T-TiO_2 (500 °C) and (b) T-TiO_2 (700 °C) thermal electrodes and (c) P-TiO_2 (500 °C) and (d) P-TiO2 (700 °C) particulate electrodes.

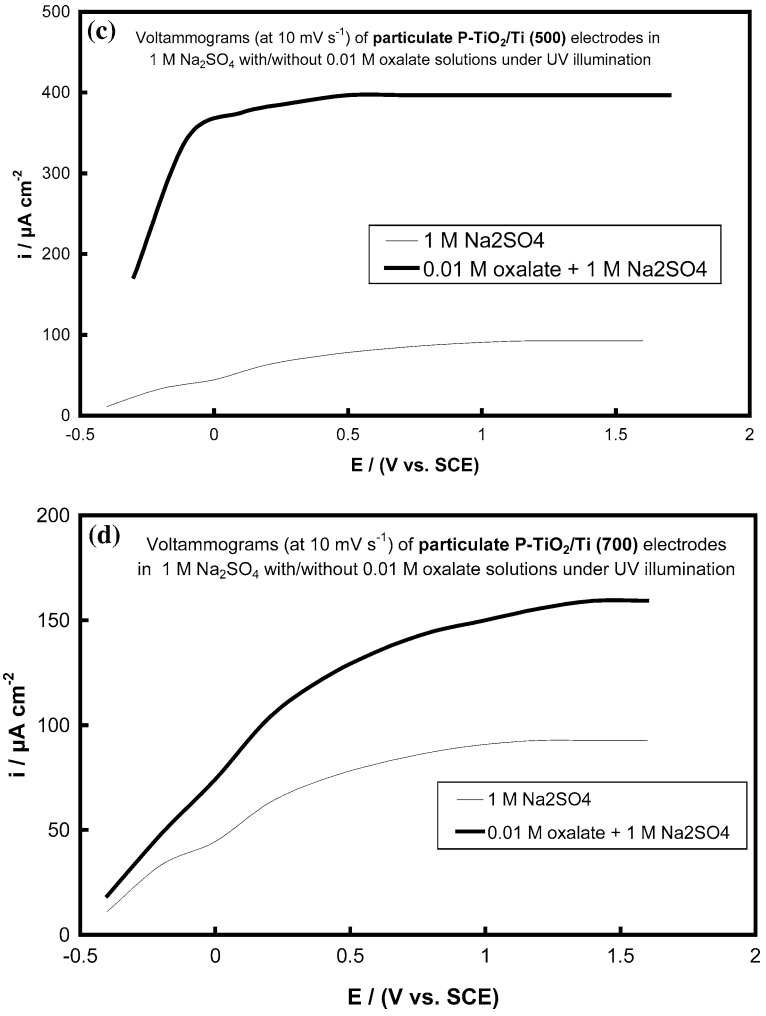

Fig. 5. Continued.

enhancement factor, F, defined as the ratio of the photocurrent in the presence of the organic divided by that in the supporting electrolyte alone. From Table 1, the above-mentioned trends can be readily identified and the significantly high value of $F = 5.09$ for the P-TiO_2 (500 °C) electrode is in line with similar data for other anatase-rich particulate electrodes reported [22, 42]. It should be stressed that the fact that the photocurrent of thermal electrodes does not increase in the presence of organics does not necessarily mean that these are less efficient in organics degradation; if all the $OH^{\cdot}$ produced at thermal electrodes is consumed for the indirect oxidation of the organics then these electrodes could be equally effective with particulate electrodes of the same photocurrent levels. In that case, the total photocurrent would be important. Figure 6 compares the photovoltammograms in 0.01 M oxalate for all electrodes and Table 1 gives data from which the trend of the photocurrent density per nominal area at + 1.7 V vs. SCE in the presence of oxalate, can be derived:

$$\text{T-TiO}_2(700\ ^\circ\text{C}) > \text{P-TiO}_2(500\ ^\circ\text{C}) > \text{T-TiO}_2(500\ ^\circ\text{C}) \approx \text{P-TiO}_2(700\ ^\circ\text{C}). \quad (6)$$

If one takes into account the photocurrent density per electroactive area (in an attempt to remove the effect of electrode surface morphology-area) then the above trend is modified as:

$$\text{T-TiO}_2(700\ ^\circ\text{C}) > \text{T-TiO}_2(500\ ^\circ\text{C}) > \text{P-TiO}_2(500\ ^\circ\text{C}) > \text{P-TiO}_2(700\ ^\circ\text{C}), \quad (7)$$

i.e. the thermal electrodes have an inherent tendency to give higher total photocurrents also in the presence of organics.

A simple and popular model for many heterogeneous photochemical oxidations is that of Langmuir–Hinshelwood kinetics (reaction of surface entities, [43]). The exact photochemical mechanism is usually more complicated: adsorbed organics can react either directly with holes or with adsorbed $OH^{\cdot}$ radicals resulting from surface-bound –OH oxidation by holes; adsorbed organics can exist as different surface complexes; "current-doubling" effects (i.e. electron injection by the initial oxidation product to the conduction band) may take place [40, 41]. However, even in those cases, kinetic equations similar to those of the

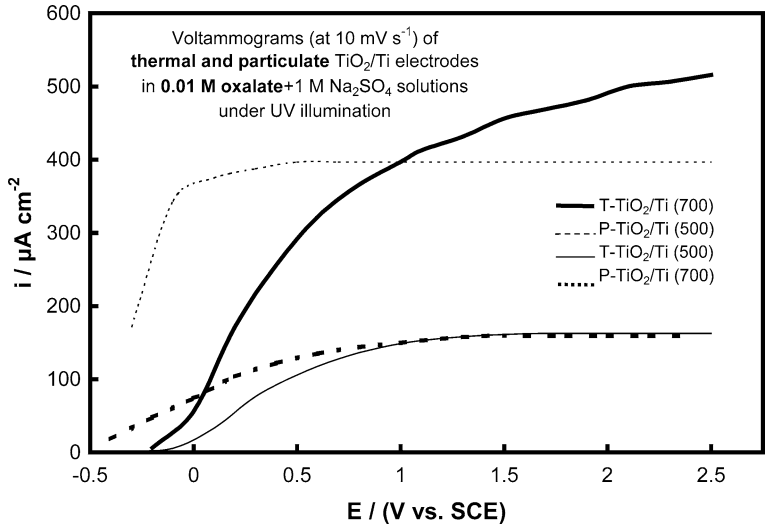

Fig. 6. Photovoltammograms of thermal and particulate TiO_2/Ti electrodes (as indicated in the graph) recorded at a 10 mV s^{-1} potential scan rate under UV illumination, in deaerated solutions of 0.01 M oxalate + 1 M Na_2SO_4.

Langmuir–Hinshelwood model may still adequately describe the photo-oxidation kinetics, their constants having an empirical rather than a mechanistic meaning. The following of Langmuir–Hinshelwood type kinetics in photoelectrocatalysis is tested by the linearity of the C/i_{ph} vs. C plot, where C is the concentration of oxalate and i_{ph} the photocurrent density at +1.7 V vs. SCE. Figure 7 presents such curves for the particulate electrodes (which are the ones showing significant photocurrent dependence on oxalate concentration) and reasonable linearity can be seen.

3.3.3. *Bulk photo-oxidation of oxalate at UV-illuminated Ti/TiO_2 electrodes*

To evaluate the activity of the electrodes for the photooxidation of oxalate, long-term constant potential bulk photo-oxidation experiments were carried out, using electrodes in the 100 cm^2 range and 300 ml 0.001 M oxalate (+1 M Na_2SO_4) solutions. The potential was kept constant at +1.5 V vs. SCE (near-limiting current region) and the observed photocurrents were in the 5–10 mA range depending on electrode used. Figure 8(a) presents the rate of oxalate degradation per nominal electrode area for the four types of thermal and particulate electrodes used as $[\ln(C_t/C_0)]/A$ vs. t plots, where C_t and C_0 are oxalate concentrations at time t and in the beginning of the experiment (measured by permanganate titration) and A is the geometric electrode area. The extent of oxalate degradation is similar (within experimental error) for all electrodes at short times, but after 90 min it follows the trend:

$$\text{P-TiO}_2(500\ ^\circ\text{C}) \approx \text{T-TiO}_2(700\ ^\circ\text{C}) > \text{T-TiO}_2(500\ ^\circ\text{C}) > \text{P-TiO}_2(700\ ^\circ\text{C}). \quad (8)$$

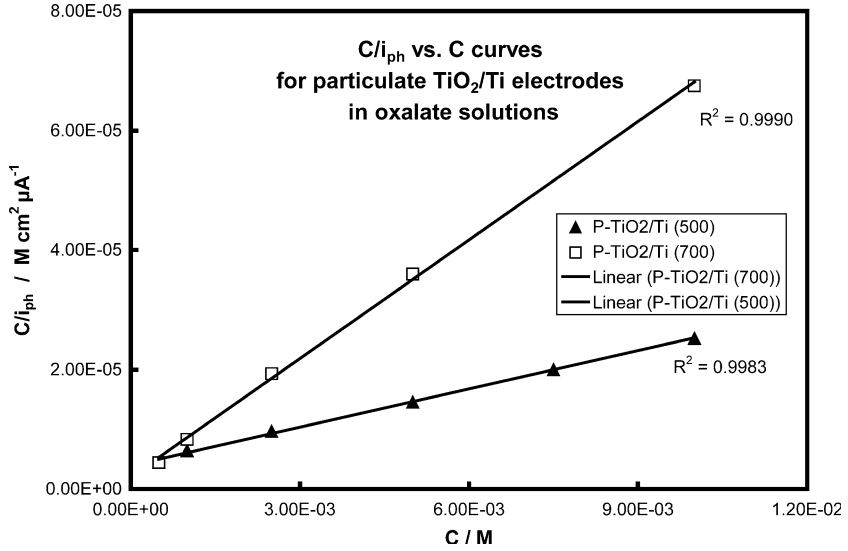

Fig. 7. Plots of the oxalate concentration to photocurrent density ratio, C/i_{ph}, vs. C for the photocurrent density at +1.7 V vs. SCE (obtained from photovoltammetric experiments under UV illumination in 1 M Na_2SO_4 solutions of varied oxalate concentration) for (a) P-TiO_2 (500 °C) and (b) P-TiO2 (700 °C) particulate electrodes.

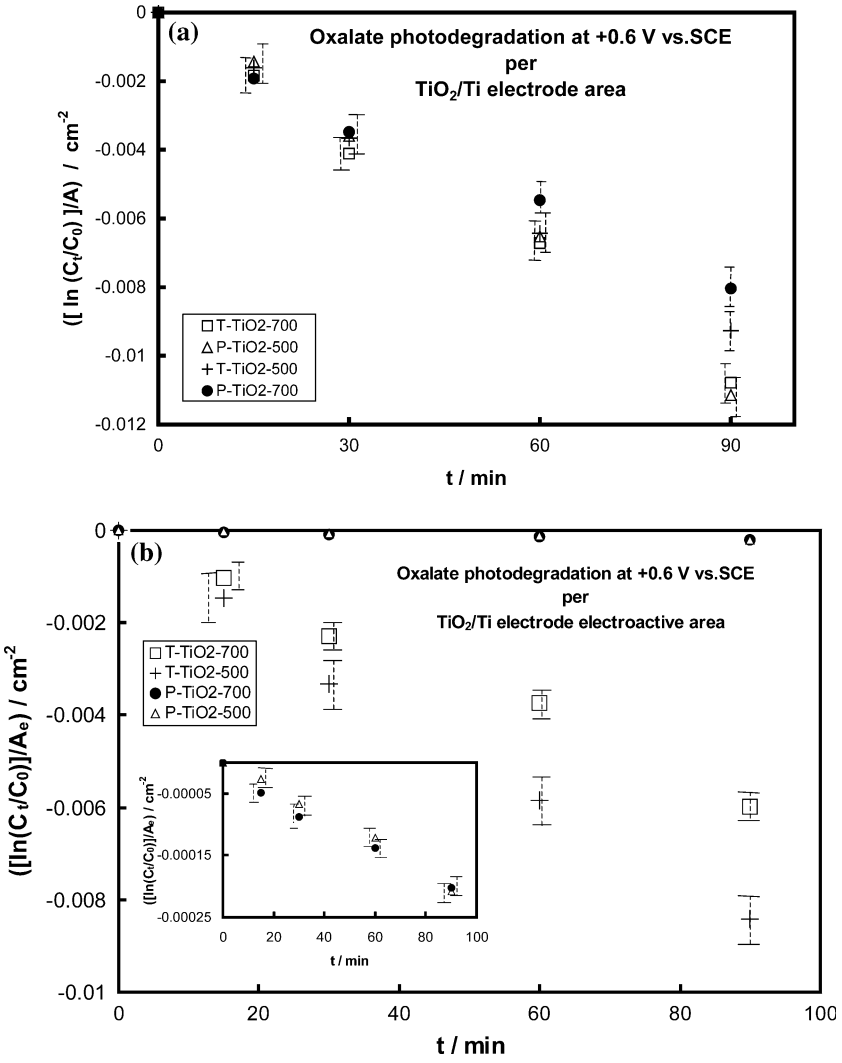

Fig. 8. Rate of oxalate degradation per electrode area during bulk photoelectrocatalysis experiments at +1.5 V vs. SCE under UV illumination in a 0.001 M oxalate + 1 M Na_2SO_4 solution for thermal and particulate electrodes (as indicated in the graph), reported as (a) $[\ln(C_t/C_0)]/A$ vs. t plots, where C_t and C_0 are oxalate concentrations at time t and in the beginning of the experiment and A is the electrode area and (b) as $[\ln(C_t/C_0)]/A_e$ vs. t plots, where A_e is the electroactive surface area. Error bars have been estimated based on a 5% error in oxalate titration.

The thermal electrode of 700 °C oxidises oxalate almost as efficiently as the particulate 500 °C electrode, despite the fact that no photocurrent enhancement is observed upon addition of oxalate for the former (see Table 1), thus excluding direct oxalate oxidation on the thermal electrode. This means that the photogenerated $OH^{\cdot}$ radicals at the T-TiO_2 (700 °C) electrode oxidise oxalate quite efficiently. Nevertheless some losses due to parallel oxygen evolution seem to occur at this electrode (i.e. lower Faradaic efficiency for oxalate oxidation) as indicated by the slight difference between the photovoltammetry trend of (6) above (where T-TiO_2 (700 °C) leads) and the oxalate degradation trend of (8) (where T-TiO_2 (700 °C) is comparable to P-TiO_2 (500 °C)).

To remove the effect of differences in catalyst surface area and focus on the influence of electrode type (thermal or particulate and anatase or rutile) on oxalate degradation rate, we report the latter with respect to the electroactive area, A_e, in Figure 8(b). The trend of (8) is then modified to:

$$\text{T-TiO}_2(500\ ^\circ\text{C}) > \text{T-TiO}_2(700\ ^\circ\text{C}) >> \text{P-TiO}_2(500\ ^\circ\text{C}) \approx \text{P-TiO}_2(700\ ^\circ\text{C}). \quad (9)$$

It can be seen that the thermal electrodes (despite their low enhancement factor, F, see Table 1) are inherently much better photoelectrocatalysts for oxalate oxidation (via indirect oxidation by $OH^{\cdot}$) than the particulate ones, presumably due to a much stronger electric field enhancement effect on continuous thermal films. Also, the anatase form of thermal electrodes seems to have a better Faradaic efficiency for oxalate oxidation than the rutile one where a parallel path of water oxidation also seems to be operative to some extent too [7, 38].

4. Conclusions

(i) The surface electrochemistry of thermal and particulate TiO_2/Ti electrodes in the dark provides a means of estimating the electroactive surface area of TiO_2 photocatalytic coatings from the charge associated with the Ti(IV)/Ti(III) transformation prior to hydrogen evolution. This area can be used to normalise photocurrents and photo-oxidation rates with respect to catalyst electroactive area and the resulting current and rate densities can then be attributed to catalyst type (thermal or particulate) or crystallographic form (anatase or rutile). This normalisation method may also be used to account for experimental surface variations between electrode specimens of the same type and form.

(ii) The photocurrent densities in plain supporting electrolyte solutions are higher for the thermal electrodes where a strong electric field enhancement effect is operative across a well-developed depletion layer within a thick uniform photocatalyst film.

(iii) The photocurrent density enhancement in the presence of the model organic of oxalate is only observed for particulate electrodes, due to their higher surface area and adsorption ability and, mainly, due to the crucial role of an organic hole scavenger in limiting the otherwise high recombination rates of particulate electrodes which lack a depletion layer.

(iv) From a practical point of view, thermal 700 °C TiO_2 electrodes (produced by simple annealing of Ti sheets) exhibit significant efficiency for oxalate photooxidation in bulk photoelectrolysis experiments, comparable to that of Degussa P-25 TiO_2 (500 °)-coated electrodes.

Acknowledgements

This work was supported by a NATO Science for Peace Project 977986 and a Greek–Cyprus bilateral research program funded by the Greek General Secretariat of Research and Technology (GSRT). The authors are indebted to E. Valova of the Institute of Physical Chemistry, Bulgarian Academy of Sciences for SEM micrographs and to Dr Ch. Lambrou, Chemical Engineering Department, Aristotle University of Thessaloniki for XRD measurements.

References

1. P.L. Yue, F. Khan and L. Rizzuti, *Chem. Eng. Sci.* **38** (1983) 1893.
2. R.W. Matthews, *J. Catal.* **111** (1988) 264.
3. S. Nishida-Yamazaki, K.J. Nagano, L.A. Phillips, S. Cervermarch and M.A. Anderson, *J. Photochem. Photobiol. A: Chem.* **70** (1993) 95.
4. I.M. Butterfield, P.A. Christensen, A. Hamnett, K.E. Shaw, G.M. Walker, S.A. Walker and C.R. Howarth, *J. Appl. Electrochem.* **27** (1997) 385.
5. R.J. Candal, W.A. Zeltner and M.A. Anderson, *J. Adv. Oxid. Technol.* **3** (1998) 270.
6. P. Fernandez-Ibanez, S. Malato and O. Enea, *Catal. Today* **54** (1999) 329.
7. P.A. Christensen, T.P. Curtis, T.A. Egerton, S.A.M. Kosa and J.R. Tinlin, *Appl. Catal. B: Environ.* **41** (2003) 371.
8. Y. Takahashi and Y. Matsuoka, *J. Mater. Sci.* **23** (1988) 2259.
9. B. O'Regan, J. Moser, M. Anderson and M. Gratzel, *J. Phys. Chem.* **94** (1990) 8720.
10. K. Kato, A. Tsuzuki, Y. Torii, H. Taoda, T. Kato and Y. Butsugan, *J. Mater. Sci.* **30** (1995) 837.
11. H. Shin, R.J. Collins, M.R. DeGurie, A.H. Heuer and C.M. Sukenik, *J. Mater. Res.* **10** (1995) 692.
12. M. Langlet, A. Kim, M. Audier, C. Guillard and J.M. Herrmann, *J. Mater. Sci.* **38** (2003) 3945.
13. L. Kavan and M. Gratzel, *Electrochim. Acta* **40** (1995) 643.
14. A.I. Martinez, D.R. Acosta and A.A. Lopez, *J. Phys.: Condens. Mater.* **16** (2004) S2335.
15. E. Fredriksson and J.-O. Carlsson, *Surf. Coat. Technol.* **73** (1995) 160.
16. E. Halary, G. Benveneti, F. Wagner and P. Hoffmann, *Appl. Surf. Sci.* **154** (2000) 146.
17. I. Zhitomirski, L. Gal-Or, A. Khon and H.W. Hennicke, *J. Mater. Sci.* **30** (1995) 5307.
18. Y. Matsumoto, Y. Ishikawa, M. Nishida and S. Ii, *J. Phys. Chem. B* **104** (2000) 4204.
19. N.J. Peill and M.R. Hoffmann, *Environ. Sci. Technol.* **29** (1995) 2974.
20. J.A. Byrne, B.R. Eggins, N.M.D Brown, B. McKinney and M. Rouse, *Appl. Catal. B: Environ.* **17** (1998) 25.
21. J. Krysa and J. Jirkovsky, *J. Appl. Electrochem.* **32** (2002) 591.
22. A. Wahl, M. Ulmann, A. Carroy and J. Augustynski, *J. Chem. Soc. Chem. Commun.* (1994) 2277.
23. A. Wahl, M. Ulmann, A. Carroy, B. Jermann, M. Dolata, P. Kedzierzawski, C. Chatelain, A. Monnier and J. Augustynski, *J. Electroanal. Chem.* **396** (1995) 41.
24. B. Parkinson, F. Decker, J.F. Juliao and M. Abramovich, *Electrochim. Acta* **25** (1979) 521.
25. M. Ulmann, N.R. Tacconi and J. Augustynski, *J. Phys. Chem.* **90** (1986) 6523.
26. V.B. Baez and D. Pletcher, *J. Electroanal. Chem.* **382** (1995) 59.
27. B.E. Hayden, D.V. Malevich and D. Pletcher, *Electrochem. Commun.* **3** (2001) 390.
28. H.O. Finklea, *in* H.O. Finklea (Ed.), Semiconductor Electrodes (Elsevier, Amsterdam, 1998), p. 57.
29. D.N. Furlong, D.E. Yates and T.W. Healy, *in* S. Trasatti (Ed.), Electrodes of Conductive Metallic Oxides (Elsevier, Amsterdam, 1981), p. 375.
30. W.W. Gardner, *Phys. Rev.* **116** (1959) 84.
31. M.A. Butler, *J. Appl. Phys.* **48** (1997) 19.
32. B. O'Regan, J. Moser and M. Gratzel, *J. Phys. Chem.* **94** (1990) 8720.
33. K. Vinodgopal, S. Hotchandani and P.V. Kamat, *J. Phys. Chem.* **97** (1993) 9040.
34. S. Sodergren, A. Hagfeldt, J. Olsson and S.-E. Lindquist, *J. Phys. Chem.* **98** (1994) 5552.
35. J. Augustynski, *in* A. Wieckowski (Ed.), Interfacial Electrochemistry: Theory, Experiment and Applications (Marcel Dekker Inc., NY, 1999), p. 707.
36. K. Vinodgopal, U. Stafford, K.A. Gray and P.V. Kamat, *J. Phys. Chem.* **98** (1994) 6797.
37. J. Krysa, M. Keppert, G. Waldner and J. Jirkovsky, *Electrochim. Acta* **50**(25–26) (2005) 5255.

38. J. Akikusa and S.U.M. Khan, *Int. J. Hydrogen Energy* **22**(9) (1997) 875.
39. T. Ohno, K. Sarukawa and M. Matsumura, *J. Phys. Chem. B* **105** (1997) 2417.
40. M.E. Calvo, R.J. Candal and S.A. Bilmes, *Environ. Sci. Technol.* **35** (2001) 4132.
41. T.L. Villareal, R. Gomez, M. Neumann-Spallart, N. Allonso-Vante and P. Salvador, *J. Phys. Chem. B* **108** (2004) 15172.
42. S. Somasundaram, N. Tacconi, C.R. Chenthamarakshan, K. Rajeshwar and N.R. de Tacconi, *J. Electroanal. Chem.* **577** (2005) 167.
43. C.S. Turchi and D.F. Ollis, *J. Catal.* **122** (1990) 1978.